# Unsteady and non-linear aeroelastic analysis of large horizontal-axis wind turbines

## Mauro S. Maza [a,b,*], Sergio Preidikman [a,b], Fernando G. Flores [a,b]

[a] CONICET — Consejo Nacional de Investigaciones Científicas y Técnicas, Argentina
[b] Departamento de Estructuras, F. de C. E. F. y N., Univ. Nac. de Córdoba, Casilla de Correo 916, 5000 Córdoba, Argentina

### ABSTRACT

Analysis results, obtained from numerical simulation, for non-linear and unsteady aeroelastic behavior of large horizontal-axis wind turbines are presented in this paper. Simulations are carried out using a partitioned scheme of weak interaction that allows dealing with the fluid—structure interaction problem by using one method to solve the structural-dynamic problem and another method for the aerodynamic problem.

The aerodynamic model used is the non-linear, unsteady vortex lattice method (NLUVLM). The structural model used is a system of beam finite elements and rigid bodies with finite rotation. This provides a very general tool with relatively low computational cost.

The proposed method allows predicting from the operating conditions (wind speed and direction, pitch angle of blades, etc.) the aeroelastic response of wind turbines, characterized by variables such as rotation speed of the rotor, loads on the structural components and the extracted power, among others.

Copyright © 2013, Hydrogen Energy Publications, LLC. Published by Elsevier Ltd. All rights reserved.

## 1. Introduction

The size of the horizontal axis wind turbines has dramatically increased in the last quarter century. They have evolved from 15 m-diameter-rotor turbines with 0.05 MW rated power to large horizontal axis wind turbines (LHAWT), commercially available today, with rotor diameters of more than 120 m and power ratios of approximately 7.5 MW [1]. This trend is expected to continue to reach turbines with rated power of about 10 MW–20 MW, which would allow, for example, to cover 20% of Europe's energy demand by 2020 and 33% by 2030 [2].

Betz's *Elementary Momentum Theory*, developed between 1922 and 1925, indicates that the maximum power extractable from an air stream by a LHAWT increases with the square of the length of the blades [3]. For this reason, the worldwide trend is to develop wind turbines with longer blades. Designs of turbines with blades of large aspect ratio and slenderness, highly flexible and constructed with composite materials, have forced to substantially change the analysis techniques. It is necessary the use of methods that are able to capture the unsteady characteristics and the nonlinearities typical of these phenomena. They must be able to represent complex constitutive relations, adequate structural damping models, coupled problems (multiphysics), etc.

The accuracy in predicting loads and the design optimization to maximize energy extraction are crucial points to

improve in order to achieve a wind turbine industry economically competitive with respect to other energy sources. The set of branches of engineering necessary to carry out an analysis of this type includes the structural dynamics and fluid mechanics, leading to the study of aeroelastic phenomena (fluid–structure interaction, FSI). The next step is the inclusion of control strategies.

The main difficulty in the field of computational aeroelasticity (CAE) is that the aerodynamic actions upon a body depend on its shape, speed, and acceleration, while these three variables depend on the aerodynamic loads of the fluid on it. To overcome this difficulty, many authors propose a partitioned scheme [4–7]. The partitioned scheme considers a phenomenon divided into sub-problems of different nature. Each sub-problem is addressed with the method that best suits it. An interaction scheme allows coupling the sub-models, thus reconstructing the original phenomenon.

This work was carried out by the same research group that led two other studies published previously. The first of these works [8] describes in detail the aerodynamic model used in the second and even the present works. The second one [9] presents an aeroelastic study, where the structure is described as a multibody system, treating the flexible bodies (tower and blades) as beams. The method of assumed-modes is used for the tower. The blades are modeled as non-straight, linearly elastic, undamped beams. Large displacements and rotations due to the motion of the blade as a rigid body are considered separately from small displacements and small rotations due to elastic deformation. In order to account for the small elastic deformation, the blades are discretized using two-noded beam finite elements along the elastic axis.

Following this line of research, the present paper incorporates the aerodynamic model presented in Ref. [8], replacing the structural model used in Ref. [9], using in this particular case nonlinear beam elements able to undergo large displacements and rotations. These elements are part of an extensive library of elements incorporated into a code of general purpose [10] that also allows modeling the nonlinear behavior of viscoelastic and anisotropic materials (essential characteristics to simulate structures built in composite materials). The existence, within that library, of shell elements would enable to improve the structural model effortlessly.

Sections 2, 3 and 4 describe the model for determining loads on the structure, the model that allows predicting the response of the structure and the scheme that interrelates both, respectively. Section 5 presents the simulation strategy and Section 6 evaluates the results. Finally, some conclusions are drawn.

## 2.    Aerodynamic model

The aerodynamic model allows determining the load of air on the blades, which causes their rotational movement and constitutes the mechanism by which the wind energy is transferred to the turbine. In this paper, we use the non-linear unsteady vortex lattice method (NLUVLM) [11]. This method shows an excellent balance between generality and computational cost. The implementation by Cristian Gebhardt for horizontal axis wind turbines LHAWT/AC [12] is used in the present effort. This method considers incompressible flow at very high Reynolds number. This allows confining vorticity to a small area of the domain within the boundary layers and the wakes, while the remainder fluid is assumed irrotational.

As a simplification, we model the boundary layer and the wake as vortex sheets. The boundary layer is represented by a vortex sheet attached to the surface of the body at all times, moving with it. Its position is determined by the displacements and deformations of the structure, and thus it represents an input for the aerodynamic problem. The wakes are represented by free vortex sheets whose positions are not specified a priori. They are convected from the sharp edges of the bodies at the local velocity of the fluid particles, taking positions so that no resultant forces act on them. These vortex sheets join at the edges where the wake is convected. Fig. 1 shows the representation of a blade and the wake associated to it.

The vortex sheets are discretized becoming aerodynamic grids (AG) composed of straight vortex segments of constant circulation $\Gamma$ along its length. Fig. 2 shows the AGs resulting from the discretization of the vortex sheets of Fig. 1. Each vortex has an associated field of perturbation velocity obtained applying the Biot–Savart Law. Two are the boundary conditions of NLUVLM: the condition of no penetration and the condition of regularity at infinity. The first one allows determining vorticity at each segment. The second is implicitly fulfilled by the Biot–Savart law.

LHAWT/AC can handle different wind directions and speed values and it can simulate the effect of the boundary layer using a pre-established velocity profile.

## 3.    Structural model

The structural model is responsible for predicting the dynamic response of the turbine to the aerodynamic loads. That is, the position, velocity and acceleration of the different parts of the machine over time. The model consists of a set of beam finite elements, rigid bodies and kinematic constraints. Simpact [10], a general purpose code with explicit integration of equations of motion, is used.
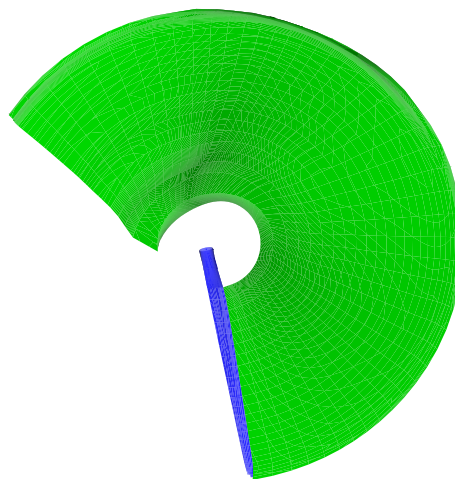


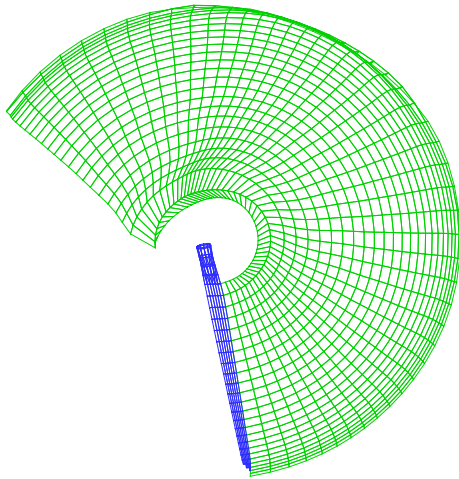Fig. 1 – **Vortex sheet representing a blade and its wake.**

**Fig. 2 — Discretization of vortex sheets in vortex grids.**

The mechanical properties of the components of the turbine have an important role in defining the structural mesh (SM): the nacelle and hub are treated as rigid bodies, while the tower and the blades are modeled as beams. The center of mass (CM) of the nacelle corresponds to the upper end of the tower and it is connected to the hub's CM through a restriction that allows rotor rotation. The roots of the blades are connected to the hub CM through rigid links that do not allow relative displacement or rotation.

The extraction of energy by the electric generator is simulated using viscous damping for the rotor rotation. This produces energy dissipation proportional to rotational speed. Gravitational forces are also included, which are essential and necessary to obtain representative results of the reality.

Currently, LHAWTs blades are constructed using composites reinforced with fibers. Fig. 3 shows an outline of a section of a typical blade made of composite material. Each pattern indicates a different material with mechanical and mass properties that are generally very dissimilar.

For adequate modeling of the blades using beam elements, it is necessary to consider the different couplings that occur due to the type of composite laminates used and the stacking sequence of these laminates in the different parts of the section of the blade.

The stiffness properties of an equivalent section must be evaluated for each generalized stress (axial, shear in both directions, torsional and bending in both directions), including the possible couplings between them. In this work PreComp [13] was used for the calculation of these stiffness properties.
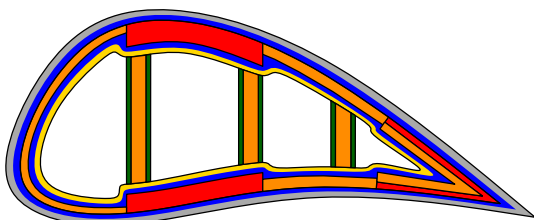


**Fig. 3 — Lamination scheme for a wind turbine blade.**

## 4. Interaction method

The interaction between the aerodynamic model and the structural/dynamic model takes place at boundary conditions level, transferring information between the AG and the SM. The displacements and velocities calculated with the structural code are used to update the position and velocity of the AG nodes. Reverse transference corresponds to the calculation of a *system of equivalent loads*, obtained from the forces provided by the NLUVLM, acting on the SM.

The method consists of an initial step that determines a structural master node, $n_m$, for each node in the AG. Furthermore, it calculates the relative position between these nodes, $r(t)$, which remain fixed throughout the entire simulation. This method is similar to that of *surface tracking* used by Cebral and Löhner [5]. The relationship between both nodes is,

$$\mathbf{x}_a(t) = \mathbf{x}_m(t) + \mathbf{r}(t).$$

Taking the time derivative of the expression above yields to the relationship that connects the velocities of these nodes as,

$$\mathbf{v}_a(t) = \mathbf{v}_m(t) + \boldsymbol{\omega}_m(t) \times \mathbf{r}_m(t)$$

where $\boldsymbol{\omega}_m(t)$ is the angular velocity vector of the structural master node.

To determine the relationship between loads, the virtual work done by the load system on the AG must be equal to that done by loads on the SM, ensuring in this way that the method does not alter artificially the total energy of the system. In this case, two relationships were obtain,

$$\mathbf{f}_m = \mathbf{f}_a, \quad \mathbf{m}_m = \mathbf{r}_m \times \mathbf{f}_a.$$

That is, applying a force on $n_a$ is equivalent to applying an equal force on $n_m$ plus a torque resulting from the translation of the original force.

Moreover, it can be shown that the method conserves the linear and angular momentum of the system. For more details, please check the reference [14].

## 5. Turbine model and simulations

### 5.1. Turbine model

The blade model used in this work is based on the data reported in Ref. [15]. It corresponds to 100 $m$-length blades entirely built in composite materials. The masses used for the nacelle and hub are determined through an up-scaling process [15]. They are: $m_n = 1.1845 \times 10^6$ kg for the nacelle and $m_h = 1.96 \times 10^5$ kg for the hub.

The tower is simulated as a beam with annular section defined by two parameters: the outer diameter and the wall thickness. These parameters are fixed at the base and upper end of the tower, and vary linearly along the tower height. Mechanical properties of typical steel are considered. The dimensions are determined so that a static/dynamic behavior of the structure in accordance to literature [3] can be obtained.

The model becomes complete after fixing two angles that define the geometry of the turbine: the *pre-tilt* angle formed by the rotor shaft and a horizontal plane, and the *pre-cone* angle,

between the blade axis and a plane normal to the rotor axis. In this study, we used values of 5° and 2.5°, respectively.

The AG has 2261 nodes and 1702 panels, while the SM, 140 nodes and 133 beam elements. These values were previously determined from the convergence analysis performed on the same turbine model. Modeling the tower and blades as beams presents the benefit that to the aerodynamic problem, the structural problem is less much expensive.

### 5.2. Simulations

Sections 6.1 and 6.2 present results for two study cases. The results corresponding to Case A are representative of the behavior of the turbine within the operation range according to reference [15]. Case B corresponds to no deformation on blades which allows analyzing the behavior of the torque applied on the rotor axis. Both cases are developed in two stages:

- Stage 1: Rotor rotation is stopped for 10 s;
- Stage 2: Rotor rotation is allowed and simulation continues up to 200 s.

For all instant $t < 0$, both gravity loads and wind speed are zero. At the beginning of the simulation, both are activated by a step function, resulting in a dynamic response that interferes with the analysis to be carried out. During the first stage, the structure reaches a static equilibrium position and the wake develops to its final length.

Figs. 4 and 5 show aerodynamic grids in both simulation stages. Fig. 4 corresponds to Stage 1. The *starting vortices* can be observed in the rear ends of wakes. Fig. 5 shows the wakes at the end of Step 2, which are helicoidal as a result of the combination of wind speed and rotation of the blades. The initial breakdown of one wake caused by its impact on the tower is also appreciated. The vectors represent the aerodynamic forces applied to the panels of the lifting surfaces.

Wind speed is the nominal speed for this turbine, 11.3 m/s, and has no lateral inclination respect to rotor rotation axis.
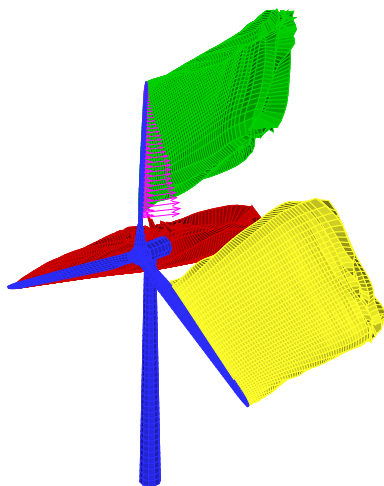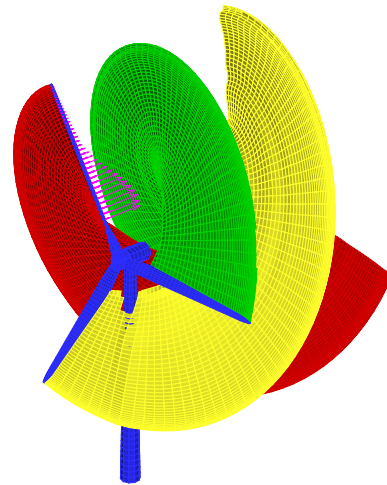


**Fig. 4 – Aerodynamic grids during Stage 1.**



**Fig. 5 – Aerodynamic grids during Stage 2.**

A value of $1 \times 10^7$ kg m$^2$/rad s is used for the viscous damping coefficient of the rotor rotational degree of freedom.

Section 6.3 shows the operating curves used to characterize the performance of this type of machines. To construct them, the data obtained from more than 50 study cases are post-processed, including those of Case A previously mentioned. In all the cases, the behavior of the turbine is studied for different values of the pitch angle of blades and wind speed.

## 6. Results

### 6.1. Global response

Fig. 6 shows the time evolution of variables along the entire simulation of Case A. The upper curve corresponds to the rotor rotation speed (hub + blades), which is zero for the first 10 $s$ and then begins to grow until it reaches a constant average value $\omega_{eq} = 0.555$ rad/s, with fluctuations with amplitudes of less than 0.2%. This is the steady state speed, and its value depends on several factors, mainly the pitch angle of blades, the free stream speed and the energy extraction.

The figure also shows the evolution of the magnitude of the aerodynamic loads acting on the blades, $F_1$, $F_2$ and $F_3$. The behavior of loads in Stage 1 is characterized by an initial peak (marked with circles on the ordinate axis), followed by a sudden drop and a number of fluctuations whose amplitudes decrease continuously until it reaches an equilibrium value.

The initial value is high (peak) due to the use of an *impulsive start*. That is, the wind speed is described as a step function that goes from 0 m/s to 11.3 m/s instantaneously at $t = 0$. At this point, vorticity concentrates on the surface of the turbine (no wake yet) and it should be enough to determine the whole velocity field around it so as to meet the no penetration condition. At the subsequent instant, the *starting vortex* is convected and loads decrease significantly.

Initial fluctuations are due to the vibrations of the flexible parts of the system (blades and tower), caused by instantaneous application of gravitational and aerodynamic loads.
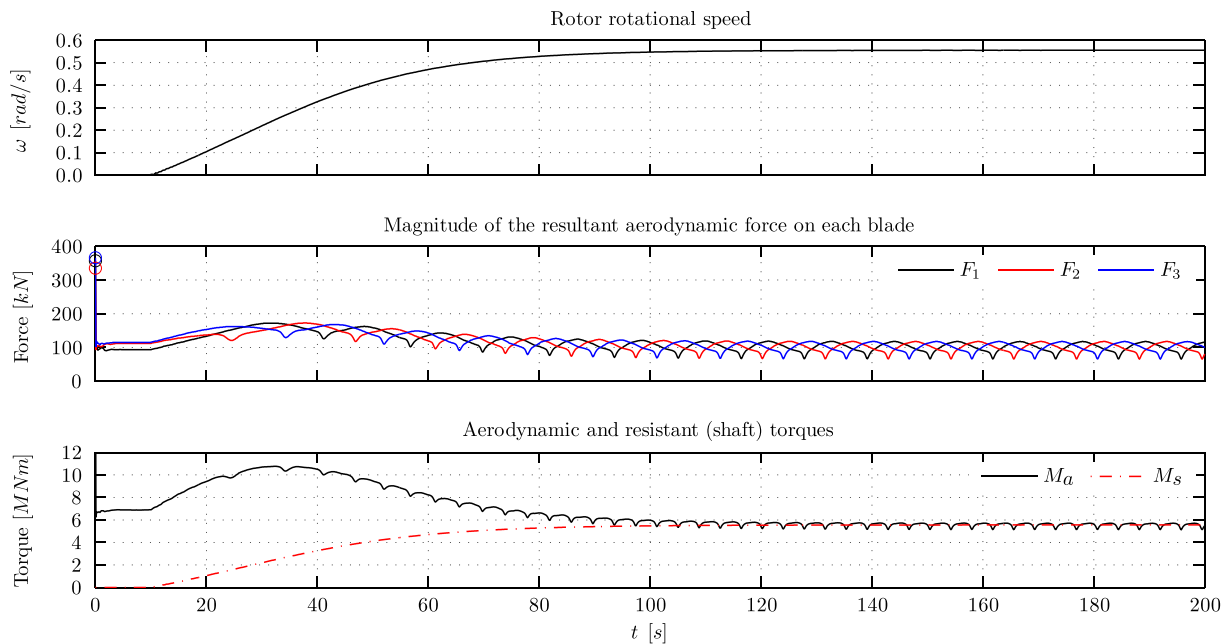
Fig. 6 – Global behavior of the turbine.

The use of large amount of damping at this stage allows quickly reaching static equilibrium.

During the second stage, periodic fluctuations of load can be observed around an average value. This value increases from the instant the rotor starts rotating freely up to a maximum value and then it suffers a slight decrease to reach a constant value. The fluctuations are the result of the aerodynamic interaction between the blades and the tower. Whenever the blades get close to the tower due to the rotor rotation, the perturbation velocity field associated to the vorticity on the tower surface produces a decrease of the aerodynamic loads on the blades.

The increase and subsequent decrease of the average value are due to a variation in rotation speed. The rotation of the rotor causes a distribution of linear velocity $\boldsymbol{v}_\omega$ on the blade sections, which is contained in the plane of rotation of the blades and whose magnitude increases linearly with the radius. This velocity, together with that of the free stream, $\boldsymbol{v}_\infty$, provides an unperturbed velocity field, $\boldsymbol{v}_u = \boldsymbol{v}_\omega + \boldsymbol{v}_\infty$, relative to each section of the blade. Not only the module of $\boldsymbol{v}_u$ varies with the rotation radius, but also the relative angle of attack at which the air reaches the blade. As a consequence, the maximum aerodynamic load is reached for a given rotation speed, which depends on the speed of the free stream and on the pitch angle of the blades. For higher rotation speed values, load reduces.

At the bottom, the evolution of the magnitudes of the aerodynamic torque, $M_a$, and the resisting torque, $M_s$, are shown. To determine $M_a$, we consider the torques, $\mathbf{M}_a^i$, that each force, $\mathbf{F}_i^j$, applied on the lifting surface produces with respect to the mass center of the hub. The torque plotted is the projection onto the rotor axis of the sum of the individual torques

$$M_a = \mathbf{t}_r \cdot \sum \mathbf{M}_a^i$$

where $\mathbf{t}_r$ is the versor coincident with the rotor axis. The time evolution of $M_a$ is totally dependent on the loads on the blades, so the same general trends can be observed.

$M_s$ is the resisting torque opposed by the electric generator on the rotor axis. In this case, it depends linearly on the rotation speed as $M_s = c\omega$, so that its evolution is equal to that of the rotor speed. The difference between $M_a$ and $M_s$ during rotor acceleration from $\omega = 0$ rad/s to $\omega_{eq}$ corresponds to the required torque to produce a speed change in the rotor. This is discussed in detail in subsection 6.2.

From $M_a$, $M_s$ and $\omega$, powers $P_a$ and $P_s$ can be calculated. The aerodynamic power, $P_a$, is a first approximation to the power extracted from the air stream. It is important to notice that its maximum value occurs, in general, at a rotation speed higher than that corresponding to the maximum values of $M_a$. This should be considered to develop control strategies to maximize the efficiency of the turbine. $P_s$ represents the electrical power generated, assuming no losses for power generation and transmission. For Case A at steady state, $P_s$ adopts a value of 3.1 MW, which represents 23% of the design rated power [15].

### 6.2. Steady state operation

We analyze in detail the steady state behavior. Fig. 7 shows the evolution of the aerodynamic torque, $M_a$, and the resisting torque, $M_s$, (left scale) and the magnitude of the aerodynamic resultant acting on the blade 1, $F_1$, (right scale) for the last three turns of the rotor. The grid corresponding to the time axis indicates, with major divisions, the duration of one complete revolution and, with secondary divisions, thirds of a turn.

The magnitude of the aerodynamic load on each blade exhibits oscillations with a period equal to the duration of one rotor turn, which is due to the aerodynamic interaction between the blades and the tower, as discussed in Subsection 6.1. Consequently, the period of $M_a$ oscillations is about one
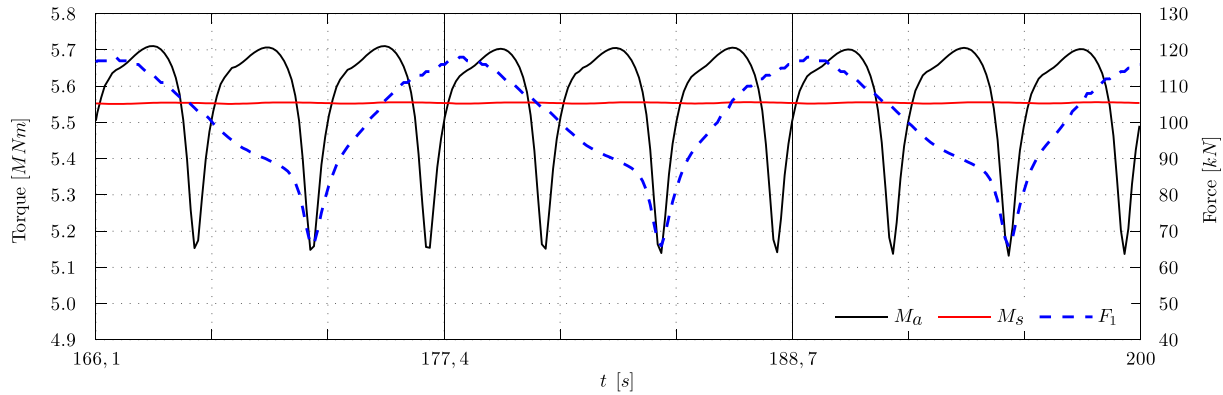
**Fig. 7 – Behavior of forces and torques in steady state operation.**

third of a turn (as it depends on the aerodynamic loads on the three blades). Such oscillations have amplitudes equal to 10.5% of the mean value, which could represent a very significant fatigue load. However, the resisting torque, $M_s$, shows very small amplitude fluctuations (less than 0.2% of mean value).

To explain this, the results for the Case B should be studied. The global behavior of the variables is very similar to those of Case A. The benefit is that, if the hub + blades system behaves as a rigid body, the equation for torque equilibrium reduces to

$$M_a = M_s + I\dot{\omega}$$

where $\dot{\omega}$ is the angular acceleration of the rotor and $I$ is the moment of inertia around the rotation axis.

In Fig. 8 are plotted the difference between torques $M_a - M_s$ and the term $I\dot{\omega}$. The curves clearly overlap, which allows to conclude the following: while the aerodynamic torque varies strongly with a frequency of three times per turn, the load torque on the rotor axis shows fluctuations of about two orders of magnitude smaller due to the large inertia of the hub + blades system, which acts as a *flywheel*, keeping the rotation speed nearly constant.

It is expected that a similar effect occurs along the entire drive train, starting from the blade surface (where the aerodynamic pressure is applied) to the rotor axis. However, this has not been studied in this work and will be the subject of future analyzes.

### 6.3. Characteristic curves

Figs. 9 and 10 correspond to the power coefficient $c_P$, and the torque coefficient, $c_Q$, respectively. On the horizontal axis, it can be observed the *advance coefficient* or *tip speed ratio*, $\lambda$. The different curves correspond to constant values of the pitch angle, $\phi$.

The advance coefficient relates the tangential speed of the blade tip due to rotor rotation speed, $v_t$, with wind speed, $v_\infty$,

$$\lambda = \frac{v_t}{v_\infty} = \frac{R\omega}{v_\infty} \tag{1}$$

where $R$ is the rotor radius.

Power and Torque coefficients are calculated as,

$$c_P = \frac{P_a}{\frac{1}{2}\rho v_\infty^3 A}, \quad c_Q = \frac{P_a}{\frac{1}{2}\rho v_\infty^2 AR}$$

where:

- $\rho$ is air density;
- $v_\infty$ is wind speed;
- A is the reference area, generally frontal area of the rotor; and
- R is the reference length, generally the rotor radius.

Using the definition of advance coefficient (1), it can be obtain an equation that relates the three non-dimensional quantities,
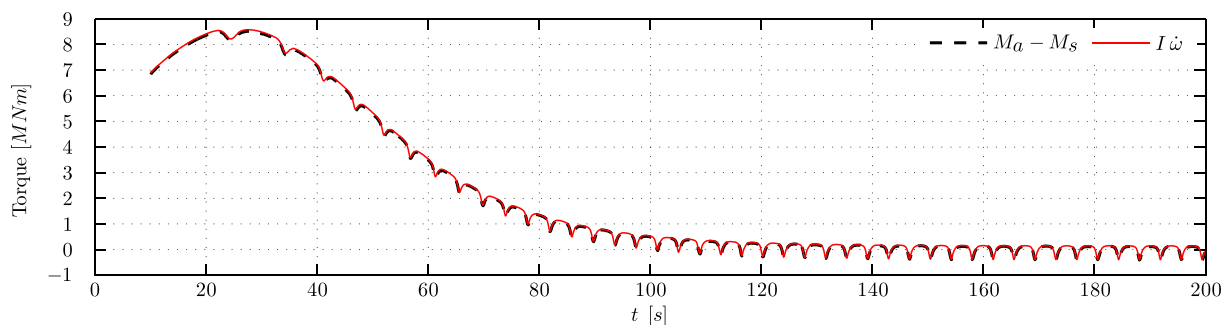


**Fig. 8 – Comparing the difference between torques $M_a - M_s$ and the rotor acceleration term for Case B (rigid blades).**
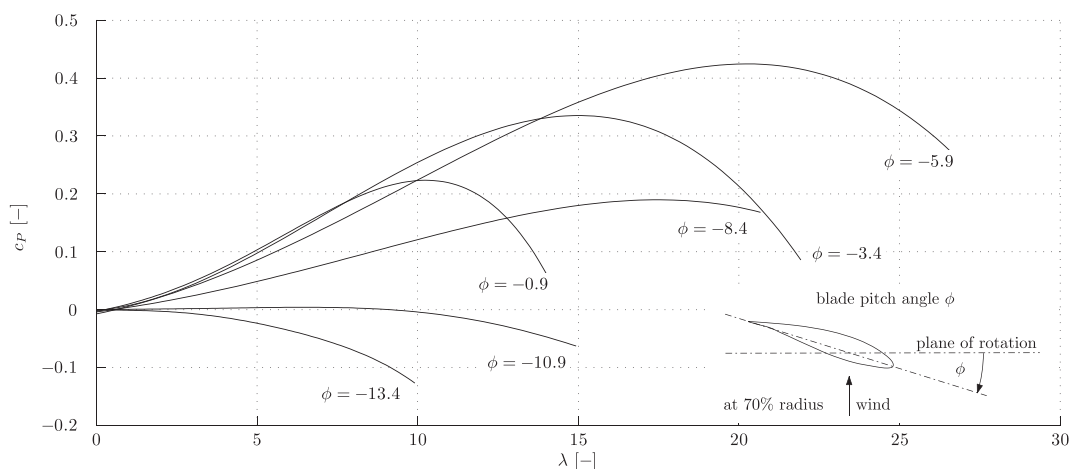
**Fig. 9 — Power coefficient $c_P$. Curves for constant pitch angle $\phi$.**

$$c_P = \lambda c_Q \qquad (2)$$

In this paper, the $c_P$ curves are determined from the power $P_a$ values obtained directly from simulation. The $c_Q$ curves were constructed as follows:

- for $\lambda > 2$, it was used the relation (2);
- for $\lambda = 0$ (that is, $\omega = 0$ rad/s), such relation is not valid, so $c_Q$ was calculated from the $M_a$ values associated to the end of Stage 1, and finally
- for $0 < \lambda < 2$, straight lines were used to join the ends of the curves with the corresponding points on the ordinate axis.

These curves characterize the performance of a particular design within its whole operation range, and allow, among other things, to evaluate the energy production capacity and to develop appropriate control strategies to ensure safe operating conditions and maximize power extraction.

## 7.    Conclusions

An interaction scheme is developed that allows coupling the *unsteady non-linear vortex lattice method* and the *finite element method*, using *non-linear finite-strain beams*. This enables studying unsteady nonlinear aeroelastic behavior of large horizontal axis wind turbines.

The method adequately captures the main phenomena of fluid—structure interaction. Globally, it includes predicting the evolution of key parameters such as rotation speed of the rotor and the generated electrical power. Locally, it is possible to capture variations of load on the blades due to aerodynamic interaction between blades and the tower.

As a significant result, the method predicts that the fluctuations of aerodynamic loads are not transmitted directly to major structural components such as the rotor axis or the anchoring structures that connect the blades to the hub. This can lead to a better estimation of fatigue loads, which represent a key factor to determine the service life of these machines.

Predictions of torque and aerodynamic power allow evaluating the overall performance of the machine at steady state operation. This information is summarized in the power and torque coefficients curves as a function of the advance coefficient, and characterize the turbine behavior.

It is expected that this method allows successfully studying unstable operating conditions, including the appearance of phenomena such as resonance or flutter, and extreme
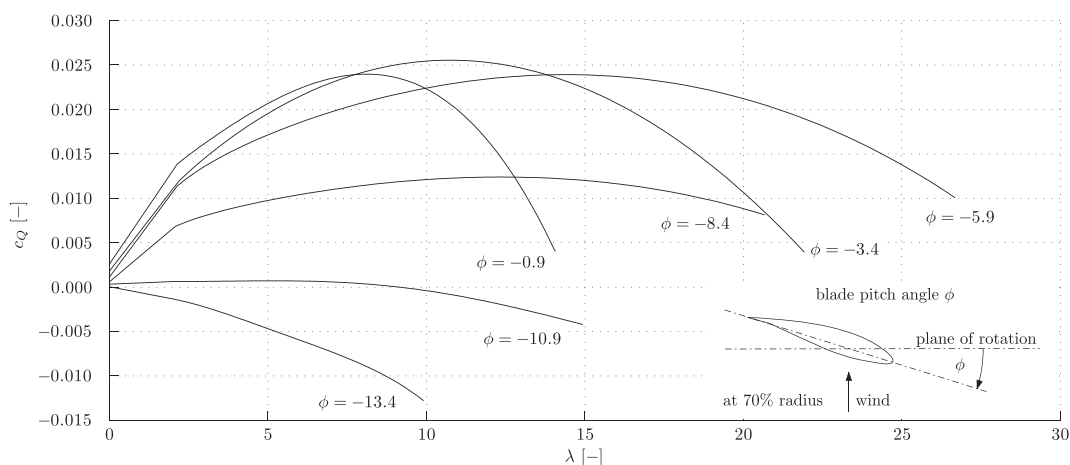


**Fig. 10 — Torque coefficient $c_Q$. Curves for constant pitch angle $\phi$.**

situations, for example excessive wind speeds or failures in the control systems.

## Acknowledgments

### REFERENCES

[1] ENERCON Web Site. E-126/7,580 kw. 2013. http://www.enercon.de/en-en/66.htm.

[2] Upwind – design limits and solutions for very large wind turbines – a 20 MW turbine is feasible. Supported by: In: The sixth framework programme for research and development of the European Commission (FP6) 2011.

[3] Hau E. Wind turbines – fundamentals, technologies, application, economics. 2nd ed. Berlin Heidelberg New York: Springer; 2005, ISBN 978-3540242406; 2005.

[4] Allen C, Rendall T. Unified approach to CFD-CSD interpolation and mesh motion using radial basis functions. In: 25th AIAA applied aerodynamics conference 2007.

[5] Cebral J, Löhner R. Conservative load projection and tracking for fluid–structure problems. AIAA J 1997;35(4):687–92.

[6] Chen P, Jadic I. Interfacing of fluid and structural models via innovative structural boundary element method. AIAA J 1998;36(2):282–6.

[7] Farhat C, Lesoinne M, Le Tallec P. Load and motion transfer algorithms for fluid–structure interaction problems with non-matching discrete interfaces: momentum and energy conservation, optimal discretization, and application to aeroelasticity. Comput Meth Appl Mech Eng 1998;157:95–114.

[8] Gebhardt CG, Preidikman S, Massa JC. Numerical simulations of the aerodynamic behavior of large horizontal-axis wind turbines. Int J Hydrogen Energy 2010;35(11):6005–11.

[9] Gebhardt CG, Preidikman S, Jrgensen MH, Massa JC. Non-linear aeroelastic behavior of large horizontal-axis wind turbines: a multibody system approach. Int J Hydrogen Energy 2012;37(19):14719–24.

[10] Flores FG. SIMPACT, an explicit finite element program. Departamento de Estructuras, U.N.C; 2011.

[11] Preidikman S. Numerical simulations of interactions among aerodynamics, structural dynamics, and control systems. Ph.D. thesis. Blacksburg, VA: Department of Engineering Science and Mechanics, Virginia Polytechnic Institute and State University; 1998.

[12] Gebhardt CG. Desarrollo de simulaciones numéricas del comportamiento aeroelástico de grandes turbinas eólicas de eje horizontal. Ph.D. thesis. Departamento de Estructuras, Facultad de Ciencias Exactas, Físicas y Naturales, Universidad Nacional de Córdoba; 2012.

[13] Bir GS. Users guide to PreComp (pre-processor for computing composite blade properties). 1617, Cole Blvd, Golden, CO 80401: National Renewable Energy Laboratory; 2005.

[14] Maza MS, Flores FG, Preidikman S. Interaccin fluido-estructura, noestacionaria y no-lineal, con modelos de flujo potencial y estructuras de vigas. Mecánica Computacional 2012;XXXI:771–95.

[15] Grifith DT, Ashwill TD. The Sandia 100-meter all-glass baseline wind turbine blade. SNL100-00. Tech. Rep. Sandia National Laboratories; 2011